Heliyon 10 (2024) e32353

Contents lists available at ScienceDirect

Heliyon

journal homepage: www.cell.com/heliyon

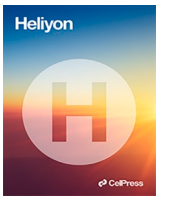

Research article

Modelling, simulation, and measurement of solar power generation: New developments in design and operational models

O. Living [a,*], S.N. Nnamchi [b], M.M. Mundu [a], K.J. Ukagwu [a], A. Abdulkarim [a], V.H.U. Eze [a]

[a] Department of Electrical, Telecom and Computer Engineering, SEAS, Kampala International University, P.O. Box 20000, Kampala, Uganda
[b] Department of Mechanical Engineering, SEAS, Kampala International University, P.O. Box 20000, Kampala, Uganda

ARTICLE INFO

Keywords:
Modelling and simulation
Solar power generation
Design and operation
Explicit and implicit models
Differential models

ABSTRACT

The discrepancy between the operating and design capacities of solar plants in eastern Uganda is alarming; about 35 % underperformance in solar power generation is observed. The goal of the current study is to minimize this disparity by improving the design models. Considering only cell temperature in the power generation model is responsible for the observed difference in design and operational solar power generated, the present study used a thermocouple to directly measure cell temperature, an anemometer to measure wind speed, and a solar power meter to measure irradiance. These extrinsic factors were used to modify the power generation model based only on cell temperature through the direct correlation of cell temperature, wind speed, and irradiance with solar power generation. Thus, the absence of extrinsic factors (wind speed and irradiance) in the design models is responsible for the colossal drop in solar power generated. Empirically, the missing extrinsic factors were used to transform the implicit solar power model into an explicit model. The development of a solar power generation model, multiple differential models, simulation and experimentation with a pilot solar rig served as alternate model for the prediction of solar power generation. The second-order differential model validated well with empirical solar power generated in Busitema, Mayuge, Soroti, and Tororo study areas based on RMSEs (0.6437, 0.6692, 0.2008, 0.1804, respectively), thus, narrowing the gap between the designed and operational solar power generated. Mayuge and Soroti recorded the highest solar power generation of 9.028 MW compared to Busitema (8.622 MW) and Tororo (8.345 MW), suggesting that it has a conducive site for installing future solar plants. The above results support the use of empirical explicit (triple) and second-order differential models for the design and operation of power plants.

Nomenclature

Abbreviation	Definition
a	Coupling coefficient
$a_i, i = 0,1,2$	Coefficients of solar power
$b_i, i = 0,1,2$	Coefficients of solar irradiance

(*continued on next page*)

* Corresponding author.
E-mail addresses: living.ounyesiga@kiu.ac.ug (O. Living), stephen.nnamchi@kiu.ac.ug (S.N. Nnamchi), mundu.mustafah@kiu.ac.ug (M.M. Mundu), ukagwu.john@kiu.ac.ug (K.J. Ukagwu), aabdulkarim@kiu.ac.ug (A. Abdulkarim), udoka.eze@kiu.ac.ug (V.H.U. Eze).

https://doi.org/10.1016/j.heliyon.2024.e32353
Received 20 January 2024; Received in revised form 12 May 2024; Accepted 3 June 2024
Available online 7 June 2024

(*continued*)

Abbreviation	Definition
$c_i, i = 0,1,2$	Coefficients of ambient temperature
$d_i, i = 0,1,2$	Coefficients of resultant wind speed
$e_i, i = 0,1,2$	Coefficients of component wind speed
ANN	Artificial neural network
cp	Specific heat capacity (kJ/kgK)
D	Dimension
d	Distance between two coordinates (km)
$\partial/\ \partial t$	Partial differential operator
$d/\ dt$	Ordinary differential operator
$D/\ Dt$	Substantial derivative operator
H	Solar irradiance (W/m^2)
e	Error in signal
MLR	Multiple linear regression
f	Mathematical function
g	Gravitational constant (m/s^2)
I	Current (A)
k	Thermal conductivity (W/mK)
MAD	Mean absolute deviation
MNSE	Modified Navier Stokes Equation
MW	Megawatt
N	Number of panels
NOCT	Nominal operating cell temperature (K)
P	Power (W, kW, MW)
$Patm$	Atmospheric pressure (kPa)
PV	Photovoltaic
$\overline{P}$	Average solar power (W, kW, MW)
r	Radius of the earth (km)
RMSE	Root mean square error
SPGMBCT	Solar power generation model based only on cell temperature
T	Temperature (K)
t	Time (s or day)
U	Wind speed (m/s)
UETCL	Uganda electricity transmission company limited
UNMA	Uganda national meteorological authority
V	Voltage (V)
X	x-maximum
x	Distance in x-direction (m or km)
Y	y-maximum
y	Distance in y-direction (m or km)
z	Distance in z-direction (m or km)
$\overline{T}$	Average temperature (K)
SD	Standard deviation.
Greek letters	
A	Thermal diffusivity (m^2/s)
B	Coefficients
X	Space vector
Φ	Latitude
H	Efficiency (%)
Λ	Longitude
P	Density (kg/m^3)
M	Dynamic viscosity (N-s/m^2 or kg/ms)
N	Kinematic viscosity (m^2/s)
Θ	Degree of implicitness
Δ	Change
Superscripts	
n	Time
◦	Degree
Subscripts	
0	Reference
1	Position one
2	Position two
$a, 0$	Ambient at reference
c	Cell
dc	Design capacity
e	Empirical
gen	Generation
i	Iteration in i
j	j-iteration
m	Measured

(*continued on next page*)

(*continued*)

Abbreviation	Definition
max	Maximum
oc	Open circuit
H	Irradiance
P	Power
p	Panel
sc	Short circuit
sim	Simulation
stc	Standard test condition
Ta	Ambient temperature
U	Wind speed
x	*x*-direction
y	*y*-direction
z	*z*-direction

1. Introduction

The performance of the PV system has been attributed to ambient conditions (temperature), cell temperature, wind speed and irradiance around the PV array. The ambient and cell temperatures are known to diminish the solar output power as the bulk of the absorbed solar power is converted into heat, which decreases the output voltage, and reduces solar power generation. Conversely, high wind speeds enhance the cooling of the PV system for optimum solar power generation. The irradiance increases power generation by increasing the output current. Besides, the efficiency of the solar cell contributes to utilizing more heat absorbed, whereby the efficiency of the solar cell is appreciable, and otherwise, the solar power generation is inhabited by the low efficiency of the solar cell. The aforementioned factors (temperature, wind speed and irradiance) could form implicit and explicit linear correlations for empirical models. In the implicit model, temperature has a direct impact on power generation, whereas wind speed and irradiance have an indirect impact on solar power generation (Chung [1], Salilih & Birhane [2], Sun [3], Sarniak [4], Al-Amri & Abdelmagid [5], Atia et al. [6], El Hammoumi et al. [7], Koehl et al. [8], Luque & Hegedus [9], Kamkird et al. [10], Alhmoud [11], Esmaeilion [12], Fenga [13], Wang [14], Esmaeilion [15]). Their pertinent findings are as follows: appropriately, Chung [1] used the nominal operating cell temperature standard model to predict insolation; however, the model could not forecast solar power generation. Suitably, Salilih & Birhane [2] applied the nominal operating cell temperature standard formula to evaluate the electrical performance of a photovoltaic system under different loads and discovered that 4 Ω recorded the highest performance. Rightly, Sun [3] developed a new nominal operating cell temperature, solar power NOCT (solar power generation model based only on cell temperature, SPGMBCT), for an unglazed photovoltaic-thermal PVT module using water as the working fluid to achieve a better prediction of SPGMBCT temperature. Precisely, Sarniak [4] presented a SPGMBCT model and discovered less power loss in half-cells relative to normal cells. Specifically, Al-Amri & Abdelmagid [5] developed a SPGMBCT model that predicts solar cell temperature in high-concentration photovoltaic systems, considering heat transfer through the materials and wind velocity. Essentially, Atia et al. [6] observed the degradation (maximum power decreases over time) of monocrystalline silicon PV modules by analyzing their performance ratio, temperature losses, and energy yield using the SPGMBCT model. Fundamentally, El Hammoumi et al. [7] examined the effect of cell temperature on the amount of energy generated on a daily basis. Precisely, Koehl et al. [8] used ambient temperature, global solar irradiation, and wind speed to develop a PV-module temperature that was validated with the measured temperature. Basically, Luque & Hegedus [9] implemented an implicit cell temperature model based on solar irradiance and operating temperature but excluded wind speed in the development of the SPGMBCT model. Primarily, Kamkird et al. [10] used temperature coefficients to modify the SPGMBCT model and achieved a good prediction of cell temperature appropriate for the design of PV systems. Principally, Alhmoud [11] attributed losses in PV systems to the nature of construction materials and suggests that proper characterization of materials improves the performance of the system. An overview of the implicit SPGMBCT model is vital in the development of the power generation model since it is found in the linear correlation model, which describes solar power generation.

Besides, the explicit empirical models are supposed to improve the prediction of cell temperature, considering that all the factors

Table 1
Design capacity of solar plants in Eastern Region of Uganda.

S#	Power Plant	Power capacity (MW)*	Lat*	Long*	2020	2021	Average data	Source
1	Busitema Solar power station	4	0.54722	34.0236	3.082	3.142	3.112	UETCL [39]
2	Busitema Solar power station (upgraded)	10	0.54722	34.0236	7.705	7.854	7.780	UETCL [39]
4	Mayuge Solar Power Station (Emerging Power – Bufulubi)	10	0.49500	33.4075	7.858	7.744	7.801	UETCL [39]
5	Soroti Solar Power Station	10	1.68500	33.6581	7.379	7.160	7.269	UETCL [39]
6	Tororo Solar North	10	0.63889	34.1192	7.205	7.247	7.226	UETCL [39]

(cell or ambient temperature, wind speed and irradiance) have a direct impact on solar power generation. The classical design/operational models of PV systems are implicit in nature; hence, the operational solar output power hardly matches the design, no matter how favorable the extrinsic factors are. The model correlation term is built solely on temperature, thus excluding wind speed and irradiance. The discrepancy is obvious from careful observation of solar power generation data from the Eastern Uganda Solar Plants (Busitema, Mayuge, Soroti and Tororo), which shows that the operational solar power generated scarcely matches the design capacities for the four plants as shown in Table 1. The discrepancy in the solar power generated compared to the design capacity calls for a remedy to minimize the difference in the design and operational solar power generation by re-engineering the design and operational models.

The re-engineering of empirical solar power generation models is advocated by the introduction of explicit power generation models; by introducing double linear correlation (Schwingshackl et al. [16], Mattei et al. [17], Olukan & Emziane [18], Nguyen et al. [19], Barykina & Hammer [20], Brito et al. [21], Sarniak [4], Ayaz et al. [22], Agyekum et al. [23], Akhsassi et al. [24], Kaldellis et al. [25], Abe et al. [26], Zouine et al. [27], Muneeshwaran et al. [28], Kalogirou [29], Cotfas et al. [30]); in retrospect, Schwingshackl et al. [16] demonstrated that incorporating wind data into the SPGMBCT models improves the prediction of cell temperature compared to standard methods. In the same manner, Mattei et al. [17], observed that the cell temperature model based on the thermal properties in lieu of wind speed or irradiance is weak in predicting cell temperature. Pertinently, Olukan & Emziane [18] modified the SPGMBCT model without the wind speed; however, they recorded a good prediction of cell temperature. Outstandingly, Nguyen et al. [19] modified the SPGMBCT model with wind speed, thermal inertia (thermal diffusivity) and irradiance to obtain a better prediction of cell temperature. In the same vein, Barykina & Hammer [20] applied the Faiman model/parameters to achieve a better prediction of cell temperature relative to the standard model. Similarly, Brito et al. [21] employed a dual explicit cell temperature model to evaluate the lifetime of PV modules and discovered more is generated by an increase in irradiance. Also, Sarniak [4] used the SPGMBCT model to investigate power losses in half-cells and normal cells and concluded that half-cells incurred less loss than normal cells. In the same manner, Ayaz et al. [22] discovered that explicit models are compatible with mono-crystalline and thin-film semiconductors.

The partial (double factors) and full (triple factors) explicit models have the capacity to minimize the difference between the design and operation of solar power generation. Uniquely, Agyekum et al. [23] investigated the impact of cooling a PV panel on its output voltage and efficiency. Exceptionally, Akhsassi et al. [24] developed multiple explicit cell temperature models, which validated well with the experimental data in a 7.2 kWp standalone photovoltaic power plant. These models engendered high precision in the module temperature without wind speed. Remarkably, Kaldellis et al. [25] examined the effect of weather conditions on the operating cell temperature and efficiency and observed that an increase in cell temperature reduces the efficiency of the panel. Distinctively, Abe et al. [26] developed a dual explicit model with the combination of irradiance and cell temperature to record good solar generation. Typically, Zouine et al. [27] and Muneeshwaran et al. [28] reviewed several implicit and explicit cell operating temperature models and found that the PV temperature significantly impacts its energy productivity. Also, Kalogirou [29] developed an explicit model of cell temperature as a function of wind speed and irradiance to calculate the efficiency of PV modules and cell temperature. In addition, Cotfas et al. [30] studied the impact of technologies on cell temperature and irradiance for commercial photovoltaic systems while measuring their current-voltage characteristics. Generally, the dual explicit SPGMBCT model gave rise to improvements in the prediction of cell temperature compared to implicit SPGMBCT models. As earlier mentioned, the application of explicit models applies to the development of solar power generation models for similar improvements in the prediction of solar power generation.

Moreover, triple linear correlation (Nguyen et al. [19], Araneo et al. [31], Skoplaki et al. [32], Kichou et al. [33], Scarabelot et al. [34], Zouine et al. [27], Muneeshwaran et al. [28], Dong et al. [35], Al-Dahidi [36], Ndegwa et al. [37]) to displace a single linear correlation in the implicit model. Significantly, Nguyen et al. [19] modified the SPGMBCT model with wind speed, thermal inertia (thermal diffusivity) and irradiance resulting in an outstanding result. Considerably, Araneo et al. [31] developed a full (triple) explicit SPGMBCT model to achieve high accuracy in cell temperature prediction. Substantially, Skoplaki et al. [32] developed explicit (triple) models based on weather, material optics, thermophysical properties, cell/ambient temperature, wind speed and irradiance, which are appropriate for the design and operation of the PV system. Outstandingly, Kichou et al. [33] discovered the impact of an explicit (triple) model on floating and land-based PVs using MATLAB simulations. Floating PV showed better performance than land PV by 3 %. Notably, Scarabelot et al. [34] used an explicit (triple) model to gain an increase in the current and solar power generated. Conspicuously, Zouine et al. [27] and Muneeshwaran et al. [28] reviewed explicit (triple) models to demonstrate the influence of cell temperature on solar power generation. Obviously, Dong et al. [35] developed a neural network to accurately predict PV cell temperature and solar power generation. Similarly, Al-Dahidi [36] developed an explicit (triple) SPGMBCT model using multiple linear regression (MLR) and artificial neural network (ANN) models for better prediction of PV cell temperature and solar power generation. Remarkably, Ndegwa et al. [37] used the explicit (triple) SPGMBCT models to achieve precision in predicting the cell temperature and solar power generation of PV systems. Based on the following findings, explicit (triple) SPGMBCT models are stronger than explicit (double) and implicit SPGMBCT models in predicting cell temperature and solar power generation for various PV technologies; hence, a triple explicit SPGMBCT model is proposed for the current study.

Further re-engineering of the solar power generation model is considered by introducing a differential (substantial derivative) solar power model, such that the solar power is a function of ambient temperature, wind speed and irradiance. The substantial derivative of solar power generation is the sum of the coupled substantial derivatives of the aforementioned trio of extrinsic factors. The substantial derivative is derived from the Navier Stokes equation by replacing the thermal and kinematic diffusivities with an electrical diffusivity and potential (the numerator of the derivatives), according to Nnamchi et al. [38]. The present work introduces first-order and

second-order substantial derivatives for modelling and simulation of solar power generation with the requisite boundary and initial conditions. A numerical solution of both differential models is sought with the finite difference method via the Crank-Nicolson explicit technique. Simulation of both numerical models will show a robust model that validates the empirical power generation data. Further validation (depicts the deviation between the simulated and measured solar power generated) of the design and empirical data is required to substantiate that the discrepancy between the design and operational data is minimized.

From the foregoing discussions on solar power generation model developments, this study develops a differential solar power generation model for the simulation of solar power generation and the development of multiple explicit empirical power generation models for improvements in the design/operations of PV systems such that the discrepancies seen in Table 1 become infinitesimal.

2. Materials and methods

2.1. Study area

Uganda, an East African landlocked nation, borders Kenya to the east, Sudan to the north, the Democratic Republic of the Congo to the west, Rwanda to the southwest, and Tanzania to the south. This study was carried out in Uganda. It consists of the following four regions: the northern, eastern, central, and western. The study was focused on the eastern region (1.2692° N, 33.4384° E) of Uganda. Due to the installation of the majority of the solar power plants, as shown in Fig. 1, the central region was chosen.

3. Methodology

The methodology consists of developing differential and empirical models for solar power generation by conducting experiments, modelling and simulations. Furthermore, field data acquired from Uganda Electricity Transmission Company Limited (UETCL), and the Uganda National Meteorological Authority (UNMA) is essential to validating the outcomes of modeling and experiments.

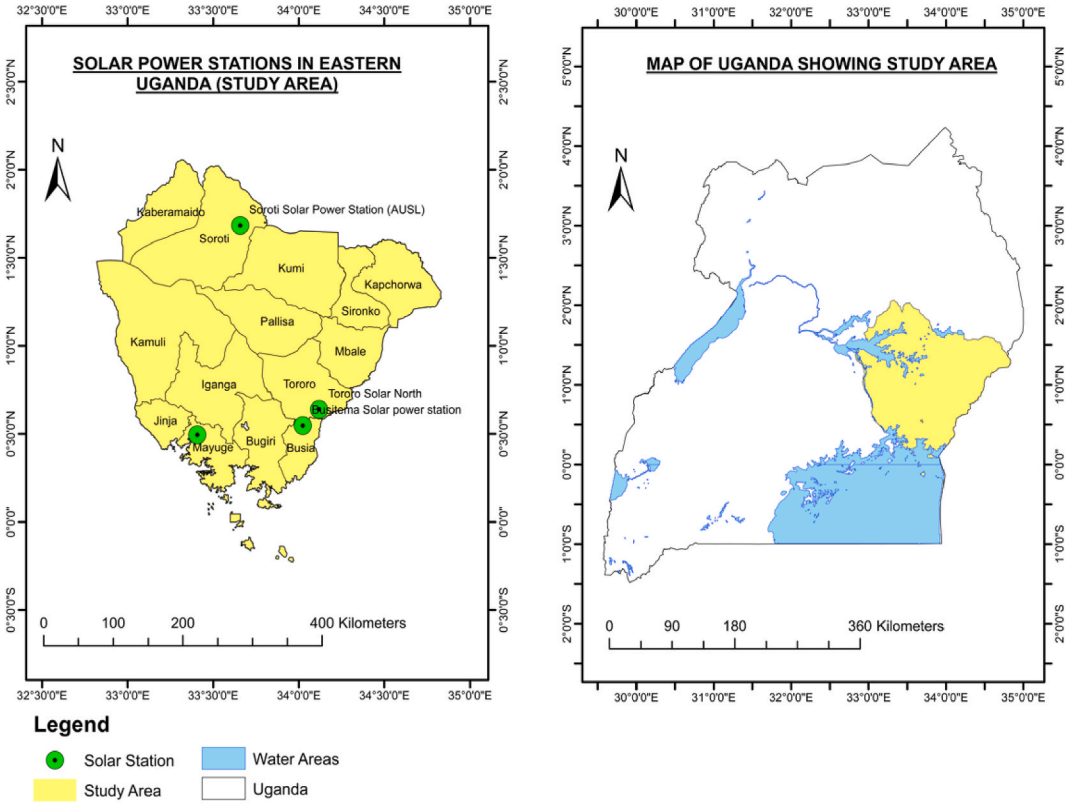

Fig. 1. Eastern region.

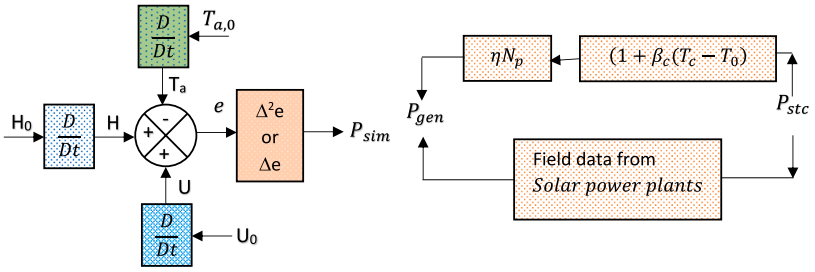

a. Solar power simulated **b**. Empirical solar power generated

Fig. 2. a. Solar power simulated. b. Empirical solar power generated.

3.1. Model formulation

Modelling and simulation, experimentation, acquisition, and analysis of data are essential for the study of solar generation, as portrayed in Fig. 2a and b. Based on simulations, solar power generation is influenced by the thermophysical characteristics of extrinsic factors such as air temperature and wind speed, as well as extraterrestrial parameters like solar irradiance. Besides, the cell temperature of the solar panel has an impact on both the formulation of solar power generation models and the empirical generation of solar power. The differential model is a balance of solar power substantial derivative against the substantial of the extrinsic factors. The field data were acquired from the existing solar power plants within the study areas (Busitema, Mayuge, Soroti, and Tororo). Where e is the error associated to the external variables, D/Dt is a substantial derivative, $H(W/m^2)$ is the solar irradiance, $U(m/s)$ is the wind speed, $P_{sim}(W)$ is the solar power simulated, $P_{gen}(W)$ is the solar power generated, $P_{stc}(W)$ is the solar power at standard test condition, $T_a(K)$ is the ambient temperature, $\beta_c(1/K)$ is the temperature coefficient of the solar cell, $\eta(\%)$ is the efficiency of solar cell, $N_p(-)$ is the number of solar panels and $T_c(K)$ is the temperature of solar cell.

3.1.1. The Navier Stokes equation

Extrinsic variables such as wind speed (U), ambient temperature (T_a), and solar irradiation (H) have an impact on photovoltaic cell performance. Hypothetically, the substantial derivatives of the Navier-Stokes equation are proposed for modeling solar power generation (Nnamchi et al. [40]. As shown in Fig. 2a and b, the wind speed is assumed to be uniform in all special coordinates, an unsteady state assumption prevails; and the pressure gradient of extrinsic factors is ignored except wind speed. Therefore, the substantial derivative of the component and resultant wind speeds are defined in Eqs. (1a), (1b) and (1c), 1d) as

$$\frac{DU_x}{Dt}=g_x-\frac{1}{\rho}\frac{\partial Patm}{\partial x}+\nu\left(\frac{\partial^2 U_x}{\partial x^2}+\frac{\partial^2 U_x}{\partial y^2}+\frac{\partial^2 U_x}{\partial z^2}\right);\ U_x=\frac{U}{\sqrt{3}};\ \nu=\mu_z\Big/\rho \tag{1a}$$

$$\frac{DU_y}{Dt}=g_y-\frac{1}{\rho}\frac{\partial Patm}{\partial y}+\nu\left(\frac{\partial^2 U_y}{\partial x^2}+\frac{\partial^2 U_y}{\partial y^2}+\frac{\partial^2 U_y}{\partial z^2}\right);\ U_y=\frac{U}{\sqrt{3}};\ \nu=\mu_z\Big/\rho \tag{1b}$$

$$\frac{DU_z}{Dt}=g_z-\frac{1}{\rho}\frac{\partial Patm}{\partial z}+\nu\left(\frac{\partial^2 U_z}{\partial x^2}+\frac{\partial^2 U_z}{\partial y^2}+\frac{\partial^2 U_z}{\partial z^2}\right);\ U_z=\frac{U}{\sqrt{3}};\ \nu=\mu_z\Big/\rho \tag{1c}$$

$$\frac{DU}{Dt}=g-\frac{U\partial U}{\partial \chi}+\nu\left(\frac{\partial^2 U}{\partial x^2}+\frac{\partial^2 U}{\partial y^2}+\frac{\partial^2 U}{\partial z^2}\right);\ \nu=\mu_z\Big/\rho;\ \chi=(xyz)^{1/3};\ U=\sqrt{3}U_x=\sqrt{3}U_y=\sqrt{3}U_z;\ Patm=0.5\rho U^2 \tag{1d}$$

Equations (1a), (1b) and (1c), 1d) are complemented with mass continuity equation in Eq. (2)

$$\frac{\partial U_x}{\partial x}+\frac{\partial U_y}{\partial y}+\frac{\partial U_z}{\partial z}=0;\ U_x=U_y=U_z=\frac{U}{\sqrt{3}} \tag{2}$$

Similarly, the substantial derivative of ambient temperature is formulated in Eq. (3)

$$\frac{DT_a}{Dt}=\alpha\left(\frac{\partial^2 T_a}{\partial x^2}+\frac{\partial^2 T_a}{\partial y^2}+\frac{\partial^2 T_a}{\partial z^2}\right);\ \alpha=k\Big/\rho cp \tag{3}$$

Likewise, the substantial derivative of solar irradiance is expressed in Eq. (4) as

$$\frac{DH}{Dt}=\alpha\left(\frac{\partial^2 H}{\partial x^2}+\frac{\partial^2 H}{\partial y^2}+\frac{\partial^2 H}{\partial z^2}\right);\ \alpha=k\Big/\rho cp \tag{4}$$

3.1.2. The Navier Stokes equation for solar power generation

The Navier-Stokes equation is a first-order substantial derivative of solar power generation in three dimensions, 3-D Nnamchi et al. [40]. It is adopted for modelling solar power generation and distribution due to its spatiality and chronological features. Integrally, solar power in Eq. (5) is a function of U, T_a and H

$$\frac{DP}{Dt}=a_H\frac{DH}{Dt}-a_{T_a}\frac{DT_a}{Dt}+a_U\frac{DU}{Dt}\;;\;\frac{DP}{Dt}=\frac{\beta_H}{\beta_P}\frac{DH}{Dt}-\frac{\beta_{T_a}}{\beta_P}\frac{DT_a}{Dt}+\frac{\beta_U}{\beta_P}\frac{DU}{Dt} \tag{5}$$

where $a_H(m^2)$, $a_{T_a}(W/K)$, $a_U(W/m/s)$ are power coupling coefficients of H, T_a and U respectively. The coupling coefficients in Eq. (5) are Defined Eq. (6) as follows:

$$a_H=\frac{\beta_H}{\beta_P};\;a_{T_a}=\frac{\beta_{T_a}}{\beta_P};\;a_U=\frac{\beta_U}{\beta_P};\;\beta_P=\frac{1}{P_{\max}}\;\;;\;\;\beta_H=\frac{1}{H_{\max}};\;\beta_{T_a}=\frac{1}{T_{a,\max}}\;\;;\;\;\beta_U=\frac{1}{U_{\max}} \tag{6}$$

Substituting substantial derivative of Eqs. (1d), (2) and (3),4) into Eq. (5) gives Eq. (7) first order linear solar power generation model.

$$\begin{aligned}\frac{\partial P}{\partial t}+U_x\frac{\partial P}{\partial x}+U_y\frac{\partial P}{\partial y}+U_z\frac{\partial P}{\partial z}=a_H\alpha\left(\frac{\partial^2 H}{\partial x^2}+\frac{\partial^2 H}{\partial y^2}+\frac{\partial^2 H}{\partial z^2}\right)-a_{T_a}\alpha\left(\frac{\partial^2 T_a}{\partial x^2}+\frac{\partial^2 T_a}{\partial y^2}+\frac{\partial^2 T_a}{\partial z^2}\right)\\+a_U\left(g-\frac{U\partial U}{\partial\chi}+\nu\left(\frac{\partial^2 U}{\partial x^2}+\frac{\partial^2 U}{\partial y^2}+\frac{\partial^2 U}{\partial z^2}\right)\right)\end{aligned} \tag{7}$$

For dominant viscous force, Eq. (7) reduces to Eq. (8)

$$\begin{aligned}\frac{\partial P}{\partial t}+U_x\frac{\partial P}{\partial x}+U_y\frac{\partial P}{\partial y}+U_z\frac{\partial P}{\partial z}=a_H\alpha\left(\frac{\partial^2 H}{\partial x^2}+\frac{\partial^2 H}{\partial y^2}+\frac{\partial^2 H}{\partial z^2}\right)-a_{T_a}\alpha\left(\frac{\partial^2 T_a}{\partial x^2}+\frac{\partial^2 T_a}{\partial y^2}+\frac{\partial^2 T_a}{\partial z^2}\right)\\+a_U\nu\left(\frac{\partial^2 U}{\partial x^2}+\frac{\partial^2 U}{\partial y^2}+\frac{\partial^2 U}{\partial z^2}\right)\end{aligned} \tag{8}$$

3.1.3. The modified Navier Stokes equation for solar power generation

The modified Navier Stokes equation is a second-order substantial derivative of solar power generation in three dimensions (3-D), also, it is adopted for modelling solar power generation and distribution due to its spatial and chronological features. Essentially, solar power in Eq. (5) is a function of U, T_a and H. Thus, an alternate power generation model (Modified Navier Stokes Equation, MNSE) is created by differentiating Eq. (5) to a second-order in Eq. (9)

$$\frac{D^2P}{Dt^2}=a_H\frac{D^2H}{Dt^2}-a_{T_a}\frac{D^2T_a}{Dt^2}+a_U\frac{D^2U}{Dt^2} \tag{9}$$

In addition, substituting second-order substantial derivative of Eqs. (1d), (2) and (3),4) into Eq. (7) gives Eq. (10)

$$\begin{aligned}\frac{D^2P}{Dt^2}=a_H\frac{D}{Dt}\left(\alpha\left(\frac{\partial^2 H}{\partial x^2}+\frac{\partial^2 H}{\partial y^2}+\frac{\partial^2 H}{\partial z^2}\right)\right)-a_{T_a}\frac{D}{Dt}\left(\alpha\left(\frac{\partial^2 T_a}{\partial x^2}+\frac{\partial^2 T_a}{\partial y^2}+\frac{\partial^2 T_a}{\partial z^2}\right)\right)\\+a_U\frac{D}{Dt}\left(\sqrt{3}\,g_x-\frac{\sqrt{3}}{\rho}\frac{\partial Patm}{\partial\chi}+\nu\left(\frac{\partial^2 U}{\partial x^2}+\frac{\partial^2 U}{\partial y^2}+\frac{\partial^2 U}{\partial z^2}\right)\right)\end{aligned} \tag{10}$$

3.1.4. Substituting substantial derivative operators in Eq. (10) yields Eq. (11)

$$\begin{aligned}\frac{D^2P}{Dt^2}=a_H\left(\alpha\left(\frac{\partial^2}{\partial x^2}+\frac{\partial^2}{\partial y^2}+\frac{\partial^2}{\partial z^2}\right)\right)\left(\alpha\left(\frac{\partial^2 H}{\partial x^2}+\frac{\partial^2 H}{\partial y^2}+\frac{\partial^2 H}{\partial z^2}\right)\right)-a_{T_a}\left(\alpha\left(\frac{\partial^2}{\partial x^2}+\frac{\partial^2}{\partial y^2}+\frac{\partial^2}{\partial z^2}\right)\right)\left(\alpha\left(\frac{\partial^2 T_a}{\partial x^2}+\frac{\partial^2 T_a}{\partial y^2}+\frac{\partial^2 T_a}{\partial z^2}\right)\right)\\+a_U\left(\frac{g}{U}-\frac{U\partial}{\partial\chi}+\nu\left(\frac{\partial^2}{\partial x^2}+\frac{\partial^2}{\partial y^2}+\frac{\partial^2}{\partial z^2}\right)\right)\left(\frac{DU}{Dt}=g-\frac{U\partial U}{\partial\chi}+\nu\left(\frac{\partial^2 U}{\partial x^2}+\frac{\partial^2 U}{\partial y^2}+\frac{\partial^2 U}{\partial z^2}\right)\right)\;;\quad Patm=0.5\rho U^2\end{aligned} \tag{11}$$

The left hand side, LHS of Eq. (11) is defined in Eq. (12)

$$\begin{aligned}\Delta^2=\frac{\partial^2 P}{\partial t^2}+2U_x\frac{\partial^2 P}{\partial x\partial t}+2U_y\frac{\partial^2 P}{\partial y\partial t}+2U_z\frac{\partial^2 P}{\partial z\partial t}+U_x^2\frac{\partial^2 P}{\partial x^2}+U_y^2\frac{\partial^2 P}{\partial y^2}+U_z^2\frac{\partial^2 P}{\partial z^2}+2U_xU_y\frac{\partial^2 P}{\partial x\partial y}\\+2U_xU_z\frac{\partial^2 P}{\partial x\partial z}+2U_yU_z\frac{\partial^2 P}{\partial y\partial z}\end{aligned} \tag{12}$$

3.1.5. Combining Eqs. 11 and 12 gives Eq. (13) solar power generation model

$$\begin{aligned}&\frac{\partial^2 P}{\partial t^2}+2U_x\frac{\partial^2 P}{\partial x\partial t}+2U_y\frac{\partial^2 P}{\partial y\partial t}+2U_z\frac{\partial^2 P}{\partial z\partial t}+U_x^2\frac{\partial^2 P}{\partial x^2}+U_y^2\frac{\partial^2 P}{\partial y^2}+U_z^2\frac{\partial^2 P}{\partial z^2}+2U_xU_y\frac{\partial^2 P}{\partial x\partial y}+2U_xU_z\frac{\partial^2 P}{\partial x\partial z}+2U_yU_z\frac{\partial^2 P}{\partial y\partial z}\\&=a_H\alpha\left(\frac{\partial^4 H}{\partial x^4}+\frac{\partial^4 H}{\partial y^4}+\frac{\partial^4 H}{\partial z^4}+2\frac{\partial^4 H}{\partial x^2\partial y^2}+2\frac{\partial^4 H}{\partial x^2\partial z^2}+2\frac{\partial^4 H}{\partial y^2\partial z^2}\right)-a_{T_a}\alpha\left(\frac{\partial^4 T_a}{\partial x^4}+\frac{\partial^4 T_a}{\partial y^4}+\frac{\partial^4 T_a}{\partial z^4}+2\frac{\partial^4 T_a}{\partial x^2\partial y^2}+2\frac{\partial^4 T_a}{\partial x^2\partial z^2}+2\frac{\partial^4 T_a}{\partial y^2\partial z^2}\right)\\&+\nu a_U\left(\begin{array}{l}\left(\frac{g^2}{U}-g\frac{\partial U}{\partial\chi}+\nu\frac{g}{U}\left(\frac{\partial^2 U}{\partial x^2}+\frac{\partial^2 U}{\partial y^2}+\frac{\partial^2 U}{\partial z^2}\right)\right)-\left(\frac{g\partial U}{\partial\chi}-\frac{U^2\partial^2 U}{\partial\chi^2}+\nu U\left(\frac{\partial^3 U}{\partial x^2\partial\chi}+\frac{\partial^3 U}{\partial y^2\partial\chi}+\frac{\partial^3 U}{\partial z^2\partial\chi}\right)\right)\\+\nu\left(\left(-\frac{U\partial^3 U}{\partial x^2\partial\chi}+\nu\left(\frac{\partial^4 U}{\partial x^4}+\frac{\partial^4 U}{\partial x^2\partial y^2}+\frac{\partial^4 U}{\partial x^2\partial z^2}\right)\right)+\left(-\frac{U\partial^3 U}{\partial y^2\partial\chi}+\nu\left(\frac{\partial^4 U}{\partial y^2\partial x^2}+\frac{\partial^4 U}{\partial y^4}+\frac{\partial^4 U}{\partial y^2\partial z^2}\right)\right)\right.\\\left.+\left(-\frac{U\partial^3 U}{\partial z^2\partial\chi}+\nu\left(\frac{\partial^4 U}{\partial x^2\partial z^2}+\frac{\partial^4 U}{\partial y^2\partial z^2}+\frac{\partial^4 U}{\partial z^4}\right)\right)\right)\end{array}\right)\end{aligned}\tag{13}$$

Similarly, considering dominant viscous force, Eq. (13) is simplified to Eq. (14)

$$\begin{aligned}&\frac{\partial^2 P}{\partial t^2}+2U_x\frac{\partial^2 P}{\partial x\partial t}+2U_y\frac{\partial^2 P}{\partial y\partial t}+2U_z\frac{\partial^2 P}{\partial z\partial t}+U_x^2\frac{\partial^2 P}{\partial x^2}+U_y^2\frac{\partial^2 P}{\partial y^2}+U_z^2\frac{\partial^2 P}{\partial z^2}+2U_xU_y\frac{\partial^2 P}{\partial x\partial y}+2U_xU_z\frac{\partial^2 P}{\partial x\partial z}+2U_yU_z\frac{\partial^2 P}{\partial y\partial z}\\&=a_H\alpha\left(\frac{\partial^4 H}{\partial x^4}+\frac{\partial^4 H}{\partial y^4}+\frac{\partial^4 H}{\partial z^4}+2\frac{\partial^4 H}{\partial x^2\partial y^2}+2\frac{\partial^4 H}{\partial x^2\partial z^2}+2\frac{\partial^4 H}{\partial y^2\partial z^2}\right)-a_{T_a}\alpha\left(\frac{\partial^4 T_a}{\partial x^4}+\frac{\partial^4 T_a}{\partial y^4}+\frac{\partial^4 T_a}{\partial z^4}+2\frac{\partial^4 T_a}{\partial x^2\partial y^2}+2\frac{\partial^4 T_a}{\partial x^2\partial z^2}+2\frac{\partial^4 T_a}{\partial y^2\partial z^2}\right)\\&+a_U\nu\left(\frac{\partial^4 U}{\partial x^4}+\frac{\partial^4 U}{\partial y^4}+\frac{\partial^4 U}{\partial z^4}+2\frac{\partial^4 U}{\partial x^2\partial y^2}+2\frac{\partial^4 U}{\partial x^2\partial z^2}+2\frac{\partial^4 U}{\partial y^2\partial z^2}\right)\end{aligned}\tag{14}$$

3.1.6. The numerical solution

Discretizing Eqs. 8 and 14 by finite the difference method to discretize solar power generated and the influential factors (H, T_a, U), leads to numerical solutions implemented in the Microsoft Excel 2013 (16.0.17029.20028) of the first and second order solar power generation models in Eqs. (15a) and (15b) and Eqs. (16a) and (16b) respectively.

$$\begin{aligned}&\frac{P_i^{n+1}-P_i^n}{\Delta t}+U_{x,i}^n\left(\theta\frac{P_{i+1}^{n+1}-P_{i-1}^{n+1}}{2\Delta x}+(1-\theta)\frac{P_{i+1}^n-P_{i-1}^n}{2\Delta x}\right)+U_{y,i}^n\left(\theta\frac{P_{i+1}^{n+1}-P_{i-1}^{n+1}}{2\Delta y}+(1-\theta)\frac{P_{i+1}^n-P_{i-1}^n}{2\Delta y}\right)\\&+U_{z,i}^n\left(\theta\frac{P_{i+1}^{n+1}-P_{i-1}^{n+1}}{2\Delta z}+(1-\theta)\frac{P_{i+1}^n-P_{i-1}^n}{2\Delta z}\right)\\&=a_H\alpha\left(\left(\frac{H_{i-1}^n-2H_i^n+H_{i+1}^n}{(\Delta x)^2}\right)+\left(\frac{H_{i-1}^n-2H_i^n+H_{i+1}^n}{(\Delta y)^2}\right)+\left(\frac{H_{i-1}^n-2H_i^n+H_{i+1}^n}{(\Delta z)^2}\right)\right)-a_{T_a}\alpha\left(\left(\frac{T_{a,i-1}^n-2T_{a,i}^n+T_{a,i+1}^n}{(\Delta x)^2}\right)\right.\\&\left.+\left(\frac{T_{a,i-1}^n-2T_{a,i}^n+T_{a,i+1}^n}{(\Delta y)^2}\right)+\left(\frac{T_{a,i-1}^n-2T_{a,i}^n+T_{a,i+1}^n}{(\Delta z)^2}\right)\right)\\&+a_U\nu\left(\left(\frac{U_{i-1}^n-2U_i^n+U_{i+1}^n}{(\Delta x)^2}\right)+\left(\frac{U_{i-1}^n-2U_i^n+U_{i+1}^n}{(\Delta y)^2}\right)+\left(\frac{U_{i-1}^n-2U_i^n+U_{i+1}^n}{(\Delta z)^2}\right)\right)\end{aligned}\tag{15a}$$

$$P_i^{n+1}=\Delta t\left(\begin{array}{l}a_H\alpha\left(H_{i-1}^n-2H_i^n+H_{i+1}^n\right)\left(\left(\frac{1}{(\Delta x)^2}\right)+\left(\frac{1}{(\Delta y)^2}\right)+\left(\frac{1}{(\Delta z)^2}\right)\right)\\-a_{T_a}\alpha\left(T_{a,i-1}^n-2T_{a,i}^n+T_{a,i+1}^n\right)\left(\left(\frac{1}{(\Delta x)^2}\right)+\left(\frac{1}{(\Delta y)^2}\right)+\left(\frac{1}{(\Delta z)^2}\right)\right)\\+a_U\nu\left(U_{i-1}^n-2U_i^n+U_{i+1}^n\right)\left(\left(\frac{1}{(\Delta x)^2}\right)+\left(\frac{1}{(\Delta y)^2}\right)+\left(\frac{1}{(\Delta z)^2}\right)\right)+\left(\frac{P_i^n}{\Delta t}\right)-\left(U_{x,i}^n\left(\frac{P_{i+1}^n-P_{i-1}^n}{2\Delta x}\right)\right.\\\left.+U_{y,i}^n\left(\frac{P_{i+1}^n-P_{i-1}^n}{2\Delta y}\right)+U_{z,i}^n\left(\frac{P_{i+1}^n-P_{i-1}^n}{2\Delta z}\right)\right)\end{array}\right)\tag{15b}$$

Similarly, Eq. (14) is discretized in Eq. (16) as

$$\begin{aligned}
&\frac{P_i^{n+2}-2P_i^{n+1}+P_i^n}{(\Delta t)^2}+2U_{x,i}^n\left(\theta\frac{P_{i+1}^{n+1}-2P_i^{n+1}+P_{i-1}^{n+1}}{(\Delta x)(\Delta t)}+(1-\theta)\frac{P_{i+1}^n-2P_i^n+P_{i-1}^n}{(\Delta x)(\Delta t)}\right)+2U_{y,i}^n\left(\theta\frac{P_{i+1}^{n+1}-2P_i^{n+1}+P_{i-1}^{n+1}}{(\Delta y)(\Delta t)}+(1-\theta)\frac{P_{i+1}^n-2P_i^n+P_{i-1}^n}{(\Delta y)(\Delta t)}\right)\\
&+2U_{z,i}^n\left(\theta\frac{P_{i+1}^{n+1}-2P_i^{n+1}+P_{i-1}^{n+1}}{(\Delta z)(\Delta t)}+(1-\theta)\frac{P_{i+1}^n-2P_i^n+P_{i-1}^n}{(\Delta z)(\Delta t)}\right)+\left(U_{x,i}^n\right)^2\left(\theta\frac{P_{i+1}^{n+1}-2P_i^{n+1}+P_{i-1}^{n+1}}{(\Delta x)^2}+(1-\theta)\frac{P_{i+1}^n-2P_i^n+P_{i-1}^n}{(\Delta x)^2}\right)\\
&+\left(U_{y,i}^n\right)^2\left(\theta\frac{P_{i+1}^{n+1}-2P_i^{n+1}+P_{i-1}^{n+1}}{(\Delta y)^2}+(1-\theta)\frac{P_{i+1}^n-2P_i^n+P_{i-1}^n}{(\Delta y)^2}\right)+\left(U_{z,i}^n\right)^2\left(\theta\frac{P_{i+1}^{n+1}-2P_i^{n+1}+P_{i-1}^{n+1}}{(\Delta z)^2}+(1-\theta)\frac{P_{i+1}^n-2P_i^n+P_{i-1}^n}{(\Delta z)^2}\right)\\
&+2\left(U_{x,i}^nU_{y,i}^n\right)\left(\theta\frac{P_{i+1}^{n+1}-2P_i^{n+1}+P_{i-1}^{n+1}}{(\Delta x\Delta y)}+(1-\theta)\frac{P_{i+1}^n-2P_i^n+P_{i-1}^n}{(\Delta x\Delta y)}\right)+2\left(U_{x,i}^nU_{z,i}^n\right)\left(\theta\frac{P_{i+1}^{n+1}-2P_i^{n+1}+P_{i-1}^{n+1}}{(\Delta x\Delta z)}+(1-\theta)\frac{P_{i+1}^n-2P_i^n+P_{i-1}^n}{(\Delta x\Delta z)}\right)\\
&+2\left(U_{y,i}^nU_{z,i}^n\right)\left(\theta\frac{P_{i+1}^{n+1}-2P_i^{n+1}+P_{i-1}^{n+1}}{(\Delta y\Delta z)}+(1-\theta)\frac{P_{i+1}^n-2P_i^n+P_{i-1}^n}{(\Delta y\Delta z)}\right)\\
&\left(\frac{H_{i-2}^n-4H_{i-1}^n+6H_i^n-4H_{i+1}^n+H_{i+2}^n}{(\Delta x)^4}\right)+\left(\frac{H_{i-2}^n-4H_{i-1}^n+6H_i^n-4H_{i+1}^n+H_{i+2}^n}{(\Delta y)^4}\right)\\
&=a_H\alpha\left(\begin{array}{l}+\left(\dfrac{H_{i-2}^n-4H_{i-1}^n+6H_i^n-4H_{i+1}^n+H_{i+2}^n}{(\Delta z)^4}\right)\\+2\left(\dfrac{H_{i-2}^n-4H_{i-1}^n+6H_i^n-4H_{i+1}^n+H_{i+2}^n}{(\Delta x\Delta y)^2}\right)+2\left(\dfrac{H_{i-2}^n-4H_{i-1}^n+6H_i^n-4H_{i+1}^n+H_{i+2}^n}{(\Delta x\Delta z)^2}\right)\end{array}\right)\\
&+2\left(\frac{H_{i-2}^n-4H_{i-1}^n+6H_i^n-4H_{i+1}^n+H_{i+2}^n}{(\Delta y\Delta z)^2}\right)\\
&\left(\frac{T_{a,i-2}^n-4T_{a,i-1}^n+6T_{a,i}^n-4T_{a,i+1}^n+T_{a,i+2}^n}{(\Delta x)^4}\right)+\left(\frac{T_{a,i-2}^n-4T_{a,i-1}^n+6T_{a,i}^n-4T_{a,i+1}^n+T_{a,i+2}^n}{(\Delta y)^4}\right)\\
&-a_{T_a}\alpha\left(\begin{array}{l}+\left(\dfrac{T_{a,i-2}^n-4T_{a,i-1}^n+6T_{a,i}^n-4T_{a,i+1}^n+T_{a,i+2}^n}{(\Delta z)^4}\right)\\+2\left(\dfrac{T_{a,i-2}^n-4T_{a,i-1}^n+6T_{a,i}^n-4T_{a,i+1}^n+T_{a,i+2}^n}{(\Delta x\Delta y)^2}\right)+2\left(\dfrac{T_{a,i-2}^n-4T_{a,i-1}^n+6T_{a,i}^n-4T_{a,i+1}^n+T_{a,i+2}^n}{(\Delta x\Delta z)^2}\right)\end{array}\right)\\
&+2\left(\frac{T_{a,i-2}^n-4T_{a,i-1}^n+6T_{a,i}^n-4T_{a,i+1}^n+T_{a,i+2}^n}{(\Delta y\Delta z)^2}\right)\\
&+a_U\nu\left(\begin{array}{l}\left(\dfrac{U_{i-2}^n-4U_{i-1}^n+6U_i^n-4U_{i+1}^n+U_{i+2}^n}{(\Delta x)^4}\right)+\left(\dfrac{U_{i-2}^n-4U_{i-1}^n+6U_i^n-4U_{i+1}^n+U_{i+2}^n}{(\Delta y)^4}\right)+\left(\dfrac{U_{i-2}^n-4U_{i-1}^n+6U_i^n-4U_{i+1}^n+U_{i+2}^n}{(\Delta z)^4}\right)\\+2\left(\dfrac{U_{i-2}^n-4U_{i-1}^n+6U_i^n-4U_{i+1}^n+U_{i+2}^n}{(\Delta x\Delta y)^2}\right)+2\left(\dfrac{U_{i-2}^n-4U_{i-1}^n+6U_i^n-4U_{i+1}^n+U_{i+2}^n}{(\Delta x\Delta z)^2}\right)+2\left(\dfrac{U_{i-2}^n-4U_{i-1}^n+6U_i^n-4U_{i+1}^n+U_{i+2}^n}{(\Delta y\Delta z)^2}\right)\end{array}\right)
\end{aligned}\tag{16a}$$

$$P_i^{n+2}=(\Delta t)^2\left(\begin{array}{l} a_H\alpha\left(\left(H_{i-2}^n-4H_{i-1}^n+6H_i^n-4H_{i+1}^n+H_{i+2}^n\right)\left(\left(\frac{1}{(\Delta x)^4}\right)+\left(\frac{1}{(\Delta y)^4}\right)+\left(\frac{1}{(\Delta z)^4}\right)\right.\right. \\ \left.\left.+2\left(\frac{1}{(\Delta x\Delta y)^2}\right)+2\left(\frac{1}{(\Delta x\Delta z)^2}\right)+2\left(\frac{1}{(\Delta y\Delta z)^2}\right)\right)\right) \\ -a_{T_a}\alpha\left(\left(T_{a,i-2}^n-4T_{a,i-1}^n+6T_{a,i}^n-4T_{a,i+1}^n+T_{a,i+2}^n\right)\left(\left(\frac{1}{(\Delta x)^4}\right)+\left(\frac{1}{(\Delta y)^4}\right)\right.\right. \\ \left.\left.+\left(\frac{1}{(\Delta z)^4}\right)+2\left(\frac{1}{(\Delta x\Delta y)^2}\right)+2\left(\frac{1}{(\Delta x\Delta z)^2}\right)+2\left(\frac{1}{(\Delta y\Delta z)^2}\right)\right)\right) \\ +a_U\nu\left(\left(U_{i-2}^n-4U_{i-1}^n+6U_i^n-4U_{i+1}^n+U_{i+2}^n\right)\left(\left(\frac{1}{(\Delta x)^4}\right)+\left(\frac{1}{(\Delta y)^4}\right)+\left(\frac{1}{(\Delta z)^4}\right)\right.\right. \\ \left.\left.+2\left(\frac{1}{(\Delta x\Delta y)^2}\right)+2\left(\frac{1}{(\Delta x\Delta z)^2}\right)+2\left(\frac{1}{(\Delta y\Delta z)^2}\right)\right)\right)- \\ \left(\begin{array}{l} +\left(P_{i+1}^n-2P_i^n+P_{i-1}^n\right)\left(\left(\frac{2U_{x,i}^n}{(\Delta x)(\Delta t)}\right)+\left(\frac{2U_{y,i}^n}{(\Delta y)(\Delta t)}\right)+\left(\frac{2U_{z,i}^n}{(\Delta z)(\Delta t)}\right)+\left(\frac{\left(U_{x,i}^n\right)^2}{(\Delta x)^2}\right)\right) \\ +\left(P_{i+1}^n-2P_i^n+P_{i-1}^n\right)\left(\left(\frac{U_{y,i}^n}{\Delta y}\right)^2+\left(\frac{U_{z,i}^n}{\Delta z}\right)^2+\left(\frac{2\left(U_{x,i}^nU_{y,i}^n\right)}{(\Delta x\Delta y)}\right)+\left(\frac{2\left(U_{x,i}^nU_{z,i}^n\right)}{(\Delta x\Delta z)}\right)+\left(\frac{2\left(U_{y,i}^nU_{z,i}^n\right)}{(\Delta y\Delta z)}\right)\right) \end{array}\right)-\left(\frac{P_i^n}{(\Delta t)^2}\right) \end{array}\right) \tag{16b}$$

3.1.7. The boundary conditions (BC)

The boundary conditions for solar power generation were derived from the field data obtained from the existing solar plants in Eastern Uganda (Fig. 1 and Table 1) and the rest of the boundary condition data were obtained from Nnamchi et al. [40], UNMA [41] and UETCL [39] for Busitema (0.547°, 34.024°), Mayuge (0.495°, 0.495°), Soroti (1.685°, 33.658°) and Tororo (0.639°, 34.119°) study areas. These mercatorian coordinates were converted to space coordinates, considering minimum latitude, φ_{min} and longitude, λ_{min} as a reference point, with the aid of the Hervasine formula (Nnamchi [40]; Prasetya et al. [42]) in Eq. (17) as

$$d=2r\sin^{-1}\left(\sqrt{\sin^2\left(\frac{\varphi_2-\varphi_1}{2}\right)+\cos(\varphi_1)\cos(\varphi_2)\sin^2\left(\frac{\lambda_2-\lambda_1}{2}\right)}\right)\quad\exists\quad x_{i+1}=x_i+d\quad;\quad y_{i+1}=y_i+d \tag{17}$$

where $d(m)$ is the distance between two coordinates, $r(m)$is the radius of the earth, $\varphi_i, i=1,2$ is the latitude of the coordinates $\lambda_i, i=1,2$ is the longitude of the coordinates, x is the distance in x-direction and y is the distance in y-direction. The boundary conditions are developed based on the similitude of Eq. (19a) with the y coordinate equal to zero and the corresponding average value of the intrinsic and extrinsic factors as a function of the x coordinate of their corresponding field data as presented in Eqs. (18a), (18b) and (18c),18d,18e), which is further regressed as a quadratic function of x.

$$P_{i,j}^0=f(x)=a_0+a_1x+a_2x^2\equiv\overline{P}\left[\frac{1}{\left(1+\left(\frac{x}{X}\right)^2\right)^{1.2}}\right]^{\frac{1}{300}} \tag{18a}$$

$$H_{i,j}^0=f(x)=b_0+b_1x+b_2x^2\equiv\overline{H}\left[\frac{1}{\left(1+\left(\frac{x}{X}\right)^2\right)^{1.2}}\right]^{\frac{1}{300}} \tag{18b}$$

$$T_{a\,i,j}^0=f(x)=c_0+c_1x+c_2x^2\equiv\overline{T_a}\left[\frac{1}{\left(1+\left(\frac{x}{X}\right)^2\right)^{1.2}}\right]^{\frac{1}{300}} \tag{18c}$$

$$U_{i,j}^{0} = f(x) = d_0 + d_1 x + d_2 x^2 \equiv \overline{U}\left[\frac{1}{\left(1+\left(\frac{x}{X}\right)^2\right)^{1.2}}\right]^{\frac{1}{300}} \tag{18d}$$

$$U_{x,i,j}^{0} = U_{y,i,j}^{0} = U_{z,i,j}^{0} = f(x) = e_0 + e_1 x + e_2 x^2 \equiv \overline{U}_x\left[\frac{1}{\left(1+\left(\frac{x}{X}\right)^2\right)^{1.2}}\right]^{\frac{1}{300}} \tag{18e}$$

where x and y are distance in x and y coordinates, $a_i, i = 0,1,2$ are coefficients of solar power, $b_i, i = 0,1,2$ are coefficients of solar irradiance, $c_i, i = 0,1,2$ are coefficients of ambient temperature, $d_i, i = 0,1,2$ are coefficients of resultant wind speed and $e_i, i = 0,1,2$ are coefficients of component wind speed, $\overline{P}(W)$, $\overline{H}\left(W/m^2\right)$, $\overline{T}_a(K)$, $\overline{U}\,(m/s), \overline{U}_x\,(m/s)$ are the average power, solar irradiance, air temperature, and wind speed respectively.

Alternatively, the present study defines $P_{i,j}^{0}$ in Eq. (19a) as

$$P_{i,j}^{0} = f(x,y) = \left[\frac{1+\left(\frac{x}{X}\right)\left(\frac{y}{Y}\right)}{\left(1+\left(\frac{x}{X}\right)^2+\left(\frac{y}{Y}\right)^2+\left(\frac{x}{X}\right)\left(\frac{y}{Y}\right)\right)^{1.2}}\right]^{\frac{1}{300}} \quad \exists \quad X = x_{\max} = 187.62\ km\ ;\ Y = y_{\max} = 193.42\ km \tag{19a}$$

3.1.8. Initial condition

Initial conditions refer to the solar power generated in the reference year in Table 1 as stated in Eq. (19b)

$$P_{i,j}^{0}(x,y\ ;\ 0) = \overline{P} = 7.5371 \quad (MW) \quad \exists \quad t = 0, 0 \le x \le 187.62 \quad km \tag{19b}$$

3.1.9. Empirical solar power generation

The first empirical solar power model is defined in Eq. (20) by the following literature (Al-Bashir et al. [43]; Scarabelot et al. [34]; Skoplaki et al. [32]) as

$$P_{gen,1} = P_{STC}(1+\beta_c(T_c - T_0))\,\eta\,N_p \quad \exists \quad \beta_c = \frac{\left(\frac{V_m - V_{oc}}{V_m}\right)}{T_m} \tag{20}$$

where $P_{gen}(W)$ is the solar power generated, $P_{stc}(W)$ is the solar power at the standard test condition, $T_a(K)$ is the ambient temperature, $T_0(K)$ is the reference temperature, $\beta_c(1/K)$ is the temperature coefficient of the solar cell, $\eta(\%)$ is the efficiency of solar cell, $N_p(-)$ is the number of solar panels and, $T_c(K)$ is the temperature of solar cell.

However, the present work considers an additional physical factor, wind speed, which enhances the cooling of the photovoltaic panel and constitute the second empirical solar power model in Eq. (21) as

$$P_{gen,2} = P_{STC}(1+\beta_c(T_c - T_0) + \beta_u U)\eta N_p \quad \exists \quad \beta_U = \frac{\left(\frac{P_{stc} - P_m}{P_m}\right)}{U_m} \tag{21}$$

Fig. 3. Experimental set up.

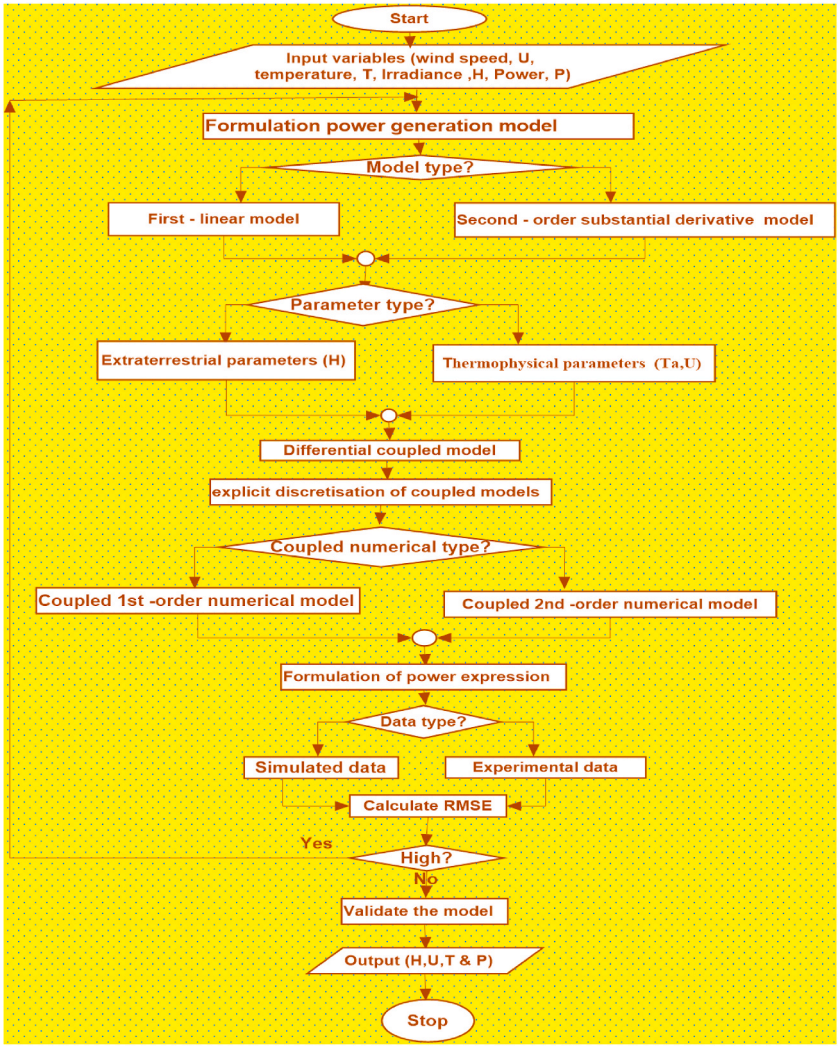

Fig. 4. Flowchart for data acquisition and power generation model.

Table 2
Empirical power generation coefficients.

S#		Coefficient	Busitema	Mayuge	Soroti	Tororo	Source
1.	Cell temperature	$\beta_c(\%^{\circ}C^{-1})$	−0.000142	−0.000157	−0.000132	−0.000351	Present study
2.	Wind speed	$\beta_u(\%sm^{-1})$	0.112316	0.135124	0.129189	0.091326	Present study
3.	Irradiance	$\beta_H\left(\%m^2W^{-1}\right)$	0.000104	0.000112	0.000067	0.000164	Present study

Table 3
Coefficients of boundary conditions.

S#	Variable	Symbol/Unit	Coefficient, $k = 0,1,2$			R^2	Source
			0	1	2		
1.	Solar power	$P^0_{i,j}(MW)$	7.5200	-4×10^{-5}	-4.0×10^{-7}	0.9985	UETCL [39]
2.	Irradiance	$H^0_{i,j}(Wm^{-2})$	684.7600	1.2320	0.0035	1.0000	Nnamchi et al. [38]
3.	Ambient temperature	$T^0_{ij}(K)$	268.9400	0.0058	3.0×10^{-5}	1.0000	UNMA [41]
4.	Resultant wind speed	$U^0_{i,j}(ms^{-1})$	0.5195	−0.0026	2.0×10^{-5}	0.9984	Nnamchi et al. [40]
5.	Component wind speed	$U^0_{x,i,j} = U^0_{y,i,j} = U^0_{z,i,j}(ms^{-1})$	0.2999	−0.0015	1.0×10^{-5}	0.9984	Nnamchi et al. [40]

These coefficients were obtained by correlating field data from UETCL [39] and Nnamchi et al. [34,36].

Table 4
Statistical description of the experimental data.

S#	Study area	Statistics	Ambient temperature ($^{\circ}C$)	Cell temperature ($^{\circ}C$)	Wind speed (m/s)	Irradiance (W/m^2)	Voltage (V)	Current (A)
1.	Busitema	Lower limit	21.20	26.50	0.00	76.40	37.60	0.12
		Mean	31.71	42.11	1.12	617.57	41.33	0.85
		Upper limit	46.70	63.80	4.14	1249.50	43.10	1.94
		SD	4.14	7.65	0.75	335.48	0.80	0.44
		MAD	3.32	6.22	0.57	302.23	0.59	0.38
2.	Mayuge	Lower limit	23.90	25.70	0.10	32.40	36.80	0.05
		Mean	32.02	41.65	0.97	588.26	41.13	0.82
		Upper limit	44.90	63.10	3.43	1382.50	43.40	1.94
		SD	3.70	9.15	0.57	353.13	0.87	0.48
		MAD	2.67	7.91	0.42	308.10	0.62	0.43
3.	Soroti	Lower limit	21.00	32.00	0.02	207.60	38.70	0.31
		Mean	28.55	44.46	0.99	717.74	41.47	1.01
		Upper limit	43.70	65.60	3.09	1331.90	44.90	2.19
		SD	3.10	6.52	0.53	348.15	1.06	0.49
		MAD	2.38	4.99	0.39	313.91	0.83	0.43
4.	Tororo	Lower limit	22.51	22.90	0.14	32.60	38.00	0.08
		Mean	29.24	44.91	1.56	682.16	41.27	1.05
		Upper limit	40.30	64.90	5.50	1314.00	43.40	2.29
		SD	3.24	10.28	0.98	343.08	1.06	0.49
		MAD	2.42	8.32	0.81	297.61	0.83	0.42

Table 5
Validation of simulated with the empirical solar power generation.

S#	Study area	Mercator coordinates		Solar power generation, P_{gen} (MW)			Root mean square error, RMSE	
		Lat.	Long.	Simulated		Empirical	$RSME_1$	$RSME_2$
				First order $P_{gen,sim1}$	Second order $P_{gen,sim2}$	$\overline{P}_{gen,emp1}$		
1.	Busitema	0.547	34.023	5.6078	7.1512	7.7818	2.1778	0.6437
2.	Mayuge	0.495	33.408	5.6075	7.1484	7.8014	2.1987	0.6692
3.	Soroti	1.685	33.658	5.6072	7.1462	7.2698	1.6701	0.2008
4.	Tororo	0.639	34.112	5.6078	7.1516	7.2190	1.6288	0.1804

Table 6
Validation of solar power design capacity with the empirical solar power generation.

S#	Study area	Mercator coordinates		Solar power generation, P_{gen} (MW)				Root mean square error, RSME		
		Lat.	Long.	Design capacity, dc	Empirical, e			$RSME_1$	$RSME_2$	$RSME_3$
				$P_{gen,dc}$	Implicit	Explicit				
					$\overline{P}_{gen,e1}$	$\overline{P}_{gen,e2}$	$\overline{P}_{gen,e3}$			
1.	Busitema	0.547	34.023	10	7.782	8.367	8.622	2.222	1.645	1.419
2.	Mayuge	0.495	33.408	10	7.801	8.419	9.028	2.199	1.587	1.023
3.	Soroti	1.685	33.658	10	7.270	7.790	8.901	2.735	2.217	1.151
4.	Tororo	0.639	34.112	10	7.232	7.780	8.345	2.772	2.227	1.683

Further modification is desired to improve the effectiveness of Eq. (19) by considering the direct influence of insolation on the output power. Third empirical solar power model is developed in Eq. (22)

$$P_{gen,3} = P_{STC}(1+\beta_c(T_c - T_0)+\beta_u U+\beta_H H)\eta N_p \quad \exists \quad \beta_H = \frac{\left(\frac{I_{sc}-I_m}{I_m}\right)}{H_m} \tag{22}$$

where the coefficients in Eqs. (18)–(20) are similarly defined in Eq. (6).

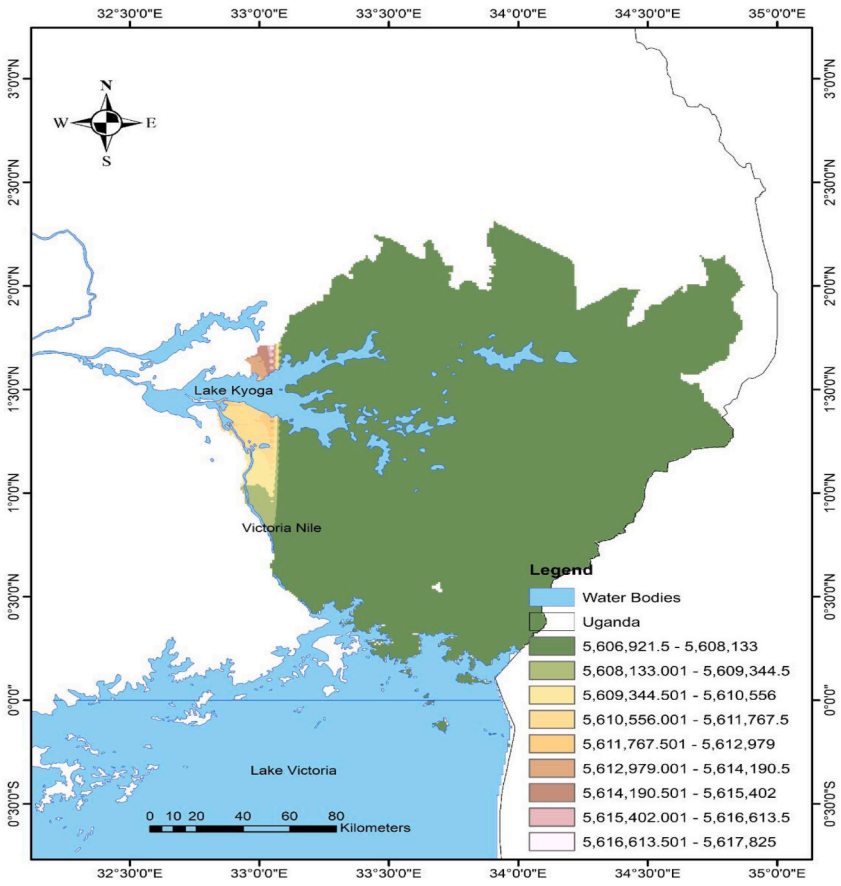

Fig. 5. Solar power generation (W) based on the first order generation model.

3.1.10. *Thermophysical properties of air*

The thermophysical properties of air are basically thermal and fluid diffusivity in Eqs. (23)–(25) and Eqs. 25 and 26 respectively, which are employed in the simulations.

The thermal conductivity is defined in Eq. (23) Nnamchi et al. [44].

$$k = 0.0121 \exp(0.0025\,\overline{T}) \quad \exists \quad \overline{T}(K) \tag{23}$$

The density, $\rho(kg/m^3)$ is expressed in Eq. (24) Nnamchi et al. [36,40] and Living et al. [45]

$$\rho_{Air} = 2.1313 - 0.003T_{Air} \quad \exists \quad 293.15 \leq T_{Air}(K) \leq 363.15, R^2 = 0.99998743 \tag{24}$$

The specific heat capacity, $cp(kJ/kgK)$ is stated in Eq. (24) Nnamchi et al. [36,40]

$$cp = 2.1313 - 0.003\overline{T} \quad \exists \quad \overline{T}(K) \tag{25}$$

The dynamic viscosity, $\mu(kg/ms)$ is stated in Eq. (24) Nnamchi et al. [36,40]

$$\mu = 1.03 \times 10^{-6} + 7 \times 10^{-8}\overline{T} - 4 \times 10^{-11}\overline{T}^2 \quad \exists \quad \overline{T}(K) \tag{26}$$

where $\overline{T}(K)$ is the average air temperature.

3.1.11. *Error analysis and validation*

Error analysis and validation of simulated and empirical, *e* solar power generation are presented in Eq. (27)

$$RMSE = \sqrt{\frac{\left(P_{gen.sim} - P_{gen.e}\right)^2}{N}} \tag{27}$$

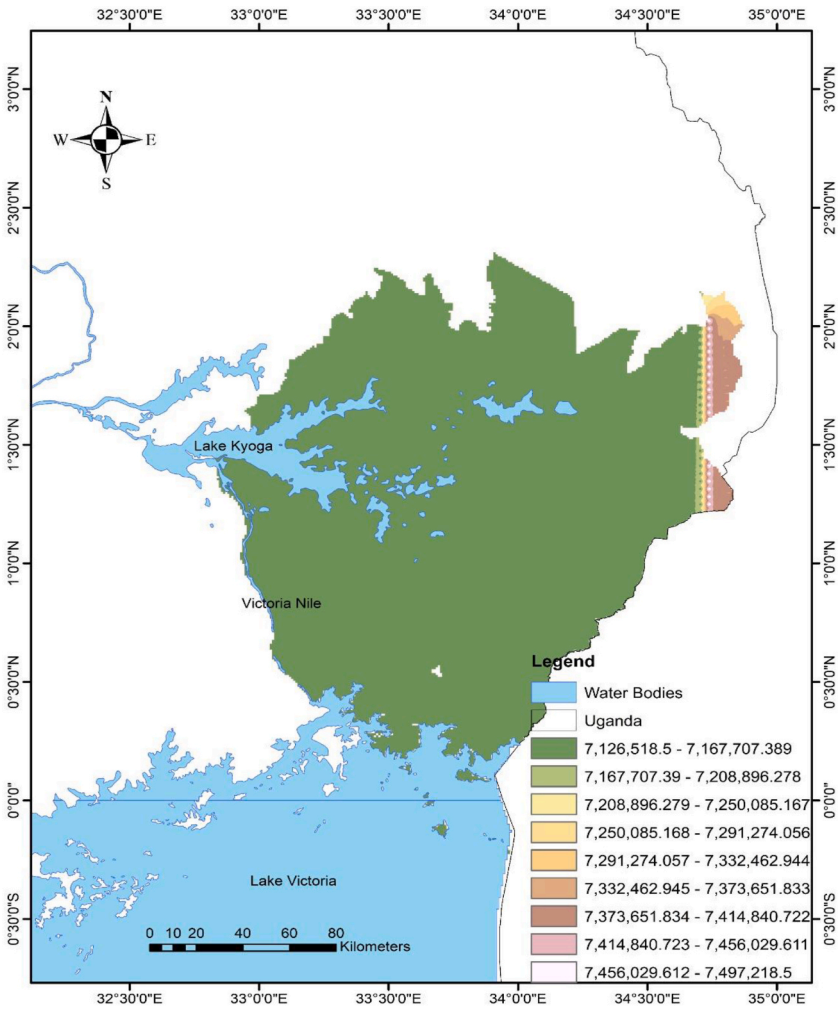

Fig. 6. Solar power generation (W) based on the second order generation model.

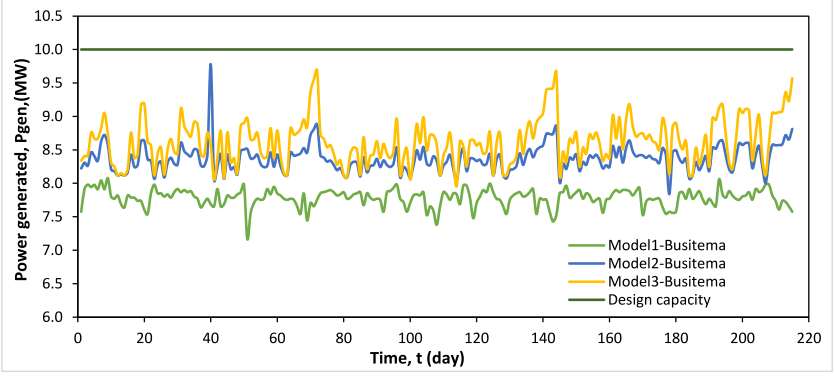

Fig. 7. Empirical solar power generation at Busitema study area.

Whereas, the error analysis and validation of design capacity, *dc* and empirical solar power generation are given in Eq. (28)

$$RMSE = \sqrt{\frac{\left(P_{gen,dc} - P_{gen,e}\right)^2}{N}} \tag{28}$$

where N is the number of observations (215), P is the solar power generated (*gen*) and subscript, *e* is the empirical power generation.

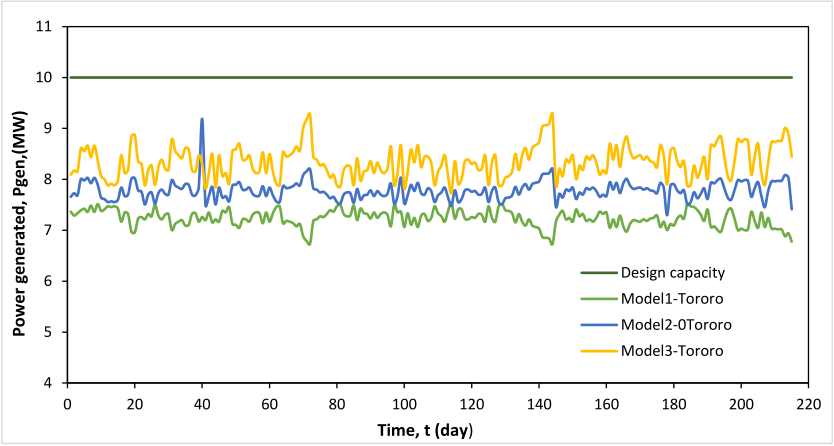

Fig. 8. Empirical solar power generation at Tororo study area.

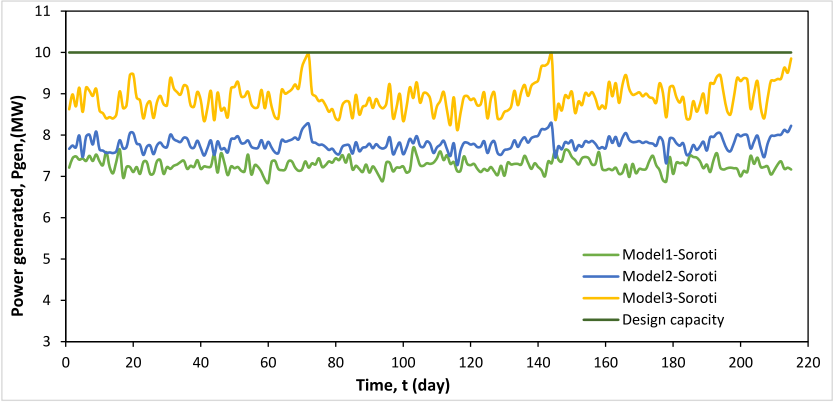

Fig. 9. Empirical solar power generation at Soroti study area.

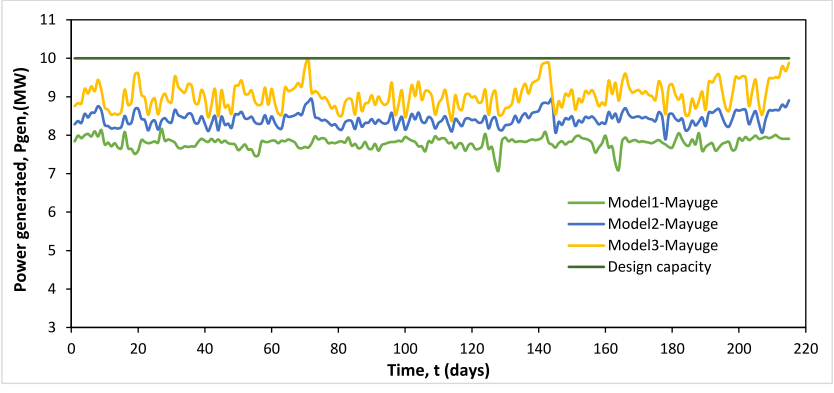

Fig. 10. Empirical solar power generation at Mayuge study area.

3.2. Experimentation

In the eastern part of Uganda, the experimental setup seen in Fig. 3 was installed next to four solar power facilities (Busitema, Mayuge, Soroti and Tororo). The set-up consisted of two ADH solar PV modules (ASO 15W–18P, +0/6.49Wp), two digital solar power meters (SM206, 0.1–1999.9 W/m^2, ±5 %), a digital multimeter (DT9205A C€, ±1 % or less), two digital thermocouples (DM6802B K-type, ±2.2 °C or ± 0.75 %) and a digital anemometer (UNI-T UT363S, 0.4–30 m/s, 10–50 °C). The following data were recorded:

ambient temperature, cell temperature, wind speed, irradiance, PV output voltage and electric current. Readings were recorded every 15 min from 09:00 a.m. to 17:00 p.m. on a daily basis. The experiment was conducted for 215 days in each study area. The algorithm in Fig. 4, explains the aforementioned methodology. The coefficients of temperature, wind speed and irradiance in Eqs. (20)–(22) and Table 2, were determined as ratios of relative voltage to temperature, relative power to wind speed and relative current to irradiance, respectively. These coefficients were used to calculate empirical solar power generation.

3.3. Description of the algorithm

The algorithm used in this work is illustrated in Fig. 4. The input data of wind speed (U), irradiance (H), temperature (T), and power (P) were acquired from (Nnamchi et al. [34,36]; UNMA [41]; UETCL [39]), respectively. Formulation of the first and second solar power generation models followed; the coefficients in the formulation are either extraterrestrial or thermophysical. Differential models of solar power generation were developed as a function of wind speed, temperature, and irradiance by coupling the aforementioned coefficients to wind speed, ambient temperature and solar irradiance. Further, explicit discretization of the differential models was carried out in order to obtain the numerical solutions of the first and second numerical models. Besides, empirical models were developed based on the experimental data and modified with the velocity; further modification with both wind speed and solar irradiance was considered. The solar power generation from simulated models was validated with empirical data. Similarly, the empirical solar generation models were validated with the design capacity of the solar power plants. Ultimately, the scheme outputted the essential results and stopped.

4. Results and discussion

4.1. Results

The results are made up of tables and figures substantiating the objectives of this study. Table 2 contains the empirical power generation coefficients; Table 3 describes the coefficients of boundary conditions; and Table 4 gives the statistical description of the experimental data. Table 5 presents the validation of simulated solar power with empirical solar power generation and Table 6 comprises the validation of solar power design capacity with empirical solar power generation.

The figures are as follows: Fig. 5 portrays the solar power generation based on the first order generation model; Fig. 6 proffers the solar power generation based on the second order model, Fig. 7 holds the empirical solar power generation at the Busitema study area and Fig. 8 depicts the empirical solar power generation at Tororo study area, Fig. 9 describes the empirical solar power generation at Soroti study area, Fig. 10 gives the empirical solar power generation at Mayuge study area, Fig. 11 shows the empirical solar power generation based on the first model for the Eastern region of Uganda; Fig. 12 illustrates the empirical solar power generation based on the second model for the Eastern region of Uganda; Fig. 13 demonstrates the empirical solar power generation based on the third model for the Eastern region of Uganda.

4.2. Discussion

This discussion is composed according to the objectives of the study and its applications.

4.2.1. Development differential models for solar power generation

Solar power generation models could be intrinsic or extrinsic models. The intrinsic model considers the generation, mobility (diffusion) and recombination of charge carriers, thus neglecting the influence of external factors (cell/ambient temperatures, wind speed and irradiance). Obviously, the impact of these factors cannot be undermined, so there is a silent need to develop a differential model that develops solar power generation as a substantial derivative of the aforementioned factors. The results in Figs. 5 and 6 present the first and second-order differential models. Validation of these results in Table 5 shows that the second order differential model validated experimental data better than the first order differential model as the RMSEs of the second order model for the study areas (Busitema, Mayuge, Soroti and Tororo) are much lower than those of the first order model. The observation could be attributed to the extended multiple spatial terms in both convective and diffusive components of the second differential model. The validation results also portrays that the boundary conditions in Eq.s (18a, 18b, 18c, 18d, 18e) and the initial condition in Eq. (19b) are precise. Consequently, the second order differential model is applicable to the global development and prediction of solar power generation in space and time (Nnamchi et al. [38]).

4.2.2. Development of empirical models for solar power generation

Empirical models are vital for ascertaining the reason behind the wide discrepancies between the design and field (operational) solar power plant capacities shown in Table 1 for the study area. The empirical model is categorized into two categories: implicit (Eq. (20)) and explicit (Eqs. 21 and 22) models. Implicit mode refers to a model with ambient/cell temperature as the only variable; hence, wind speed and irradiance have an indirect impact on solar power generation, whereas the explicit model does not encapsulate wind speed or solar irradiance, thus having a direct impact on solar power generation. Observing Figs. (7)–(10), the operational solar power generated for the implicit empirical model is far from reaching the design capacity in Table 1, and the operational solar generation data for the explicit (double), minimize the gap between the design and operational solar power capacities and operational solar power generation data for explicit (triple) much closer the gap between the design and operational solar power plant capacities. The

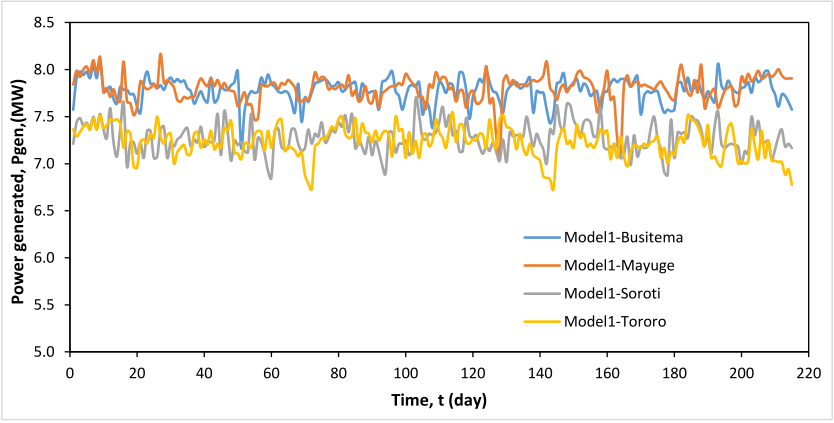

Fig. 11. Empirical solar power generation based on first model for Eastern region of Uganda.

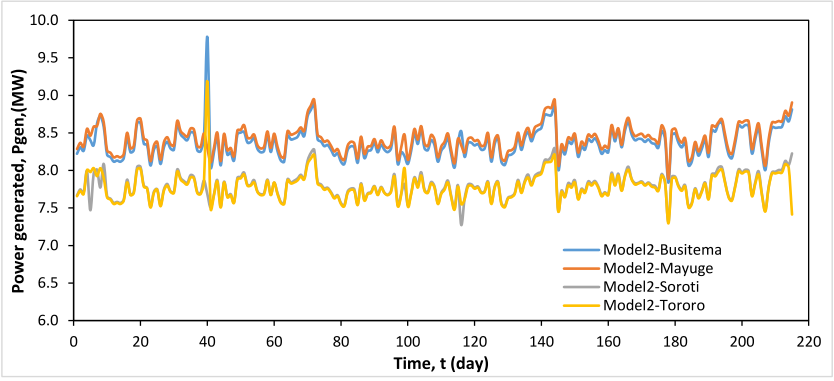

Fig. 12. Empirical solar power generation based on second model for Eastern region of Uganda.

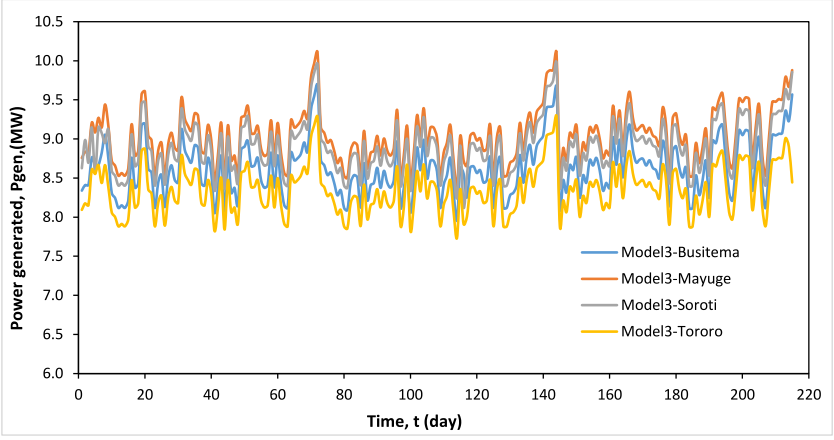

Fig. 13. Empirical solar power generation based on third model for Eastern region of Uganda.

phenomena observed in these Figs. (7)–(10), show that the implicit model is far insufficient for predicting the solar power generated as it does not have a direct impact of both wind speed and solar irradiance in its formulation (Chung [1]; Sun [3]; Sarniak [4]; Al-Amri & Abdelmagid [5]; Atia et al. [6]; El Hammoumi et al. [7]; Alhmoud [11]). Conversely, the explicit (double) in Eq. (21) has both cell temperature and wind speed directly built into the formulation, thus, it has the ability to bridge the gap between the design and operational capacities relative to the implicit model. Moreover, the explicit (triple) model in Eq. (22) is built on the three extrinsic factors (ambient/cell temperature, wind speed and irradiance) to further bridge the gap or discrepancy between the design and

operational capacities (Nguyen et al. [19]; Kichou et al. [33]; Scarabelot et al. [34]; Muneeshwaran et al. [28]; Dong et al. [35]; Al-Dahidi [36]; Ndegwa et al. [37]). However, explicit (triple) draws the operational to design capacity only when the combination of the extrinsic factors is favorable and vice versa.

Observing Figs. (11)–(13), Mayuge recorded the highest solar power generation based on model 1, model 2 and model 3 compared to other study areas. This result is supported by the RMSE analysis in Table 6, which recorded the lowest values compared to other study areas. Besides, the impact of wind speed and solar irradiance is directly accounted for in the explicit (triple) model. Future solar plants should be sited at Mayuge and Soroti as the leading sites.

4.2.3. Limitation of the models

The differential models (first and second-order) are void of truncation errors since regression analysis is not implemented in the solution, whereas the explicit and implicit empirical models have truncation errors due to the regression of these models. However, RMSEs indicate that the triple explicit empirical model showed strong agreement with the design capacity by virtue of the integrity extrinsic factor. The assumption of a uniform distribution of wind speed could not mar the results, and the application of the Navier Stokes model was suitable for modelling of solar power generation since the simulated and empirical results are in good agreement.

4.2.4. Applications of the developed models

An explicit (triple) model should be implemented in the design of solar power plants, as its sensitivity to solar power generation is very high. Both empirical (explicit-triple) and second order differential models are useful for the effective operation of solar power plants. The second differential model could compliment the empirical model in providing detailed and accurate design information in space and time.

where *MAD* implies mean absolute deviation and *SD* designates standard deviation. The detailed experimental data is found in the supplementary file.

5. Conclusions

This paper carried out modeling, simulation, and empirical studies of solar power generation with the aim of developing realistic design and operational models that minimize the gap between their capacities. The modeling encompasses differential modeling and empirical models. The differential model covers first- and second-order models for the simulation of solar power generation, whereas the empirical model comprises explicit and implicit models. The explicit models could be double or triple depending on the number of extrinsic factors. Based on the differential modeling, simulation, and validation, the second-order differential model yielded 7.1484 MW, which is in good agreement with experimental (7.8014 MW) results relative to the first-order differential model (5.6075 MW) due to the extended space terms in its formulation.

Explicit models minimized the gap between the design and operational solar power generation capacities. However, the explicit triple model performed better than the explicit double model due to more extrinsic factors directly impacting solar power generation. It was observed that both the implicit (7.801 MW) and explicit (8.419 − 9.028 MW) models worked well for Mayuge and Soroti when compared to other study areas (Busitema and Tororo). This result signifies that solar power generation in Mayuge and Soroti is favored by extrinsic factors (ambient temperature, wind speed and solar irradiance). If the extrinsic factors are not favorable, the discrepancy between the design and operational solar power generation remains imminent.

Therefore, this work recommends the use of a second-order differential model and an explicit triple model for universal prediction of solar power generation. Also, the models could be implemented in the design of solar power plants with high performance since both extrinsic and intrinsic factors are integrated into the models. Furthermore, the combined impacts of extrinsic factors on solar power generation models should be considered for improving operational and design models.

Data availability

The data used in this research will be made available on request.

CRediT authorship contribution statement

O. Living: Writing – review & editing, Writing – original draft, Formal analysis, Conceptualization. **S.N. Nnamchi:** Supervision. **M. M. Mundu:** Supervision. **K.J. Ukagwu:** Supervision. **A. Abdulkarim:** Supervision. **V.H.U. Eze:** Supervision.

Declaration of competing interest

The authors declare that they have not known competing financial interests or personal relationships that could have appeared to influence the work reported in this study.

Acknowledgements

The authors would like to acknowledge the Uganda Electricity Transmission Company Limited, UETCL, and the Uganda National Meteorological Authority, UNMA, for providing the data used in the study.

References

[1] M.H. Chung, Estimating solar insolation and power generation of photovoltaic systems using previous day weather data, Adv. Civ. Eng. (2020) 1–13, https://doi.org/10.1155/2020/8701368. Article ID 8701368.
[2] E.M. Salilih, Y.T. Birhane, Modeling and analysis of photo-voltaic solar panel under constant electric load, J. Renew. Energy (2019) 10, https://doi.org/10.1155/2019/9639480. Article ID 9639480.
[3] V. Sun, A. Asanakham, T. Deethayat, T. Kiatsiriroat, A new method for evaluating nominal operating cell temperature (NOCT) of unglazed photovoltaic thermal module, Energy Rep. 6 (2020) 1029–1042, https://doi.org/10.1016/j.egyr.2020.04.026.
[4] M.T. Sarniak, Modeling the functioning of the half-cells photovoltaic module under partial shading in the matlab package, Appl. Sci. 10 (7) (2020) 2575, https://doi.org/10.3390/app10072575.
[5] F.G. Al-Amri, T.I.M. Abdelmagid, Analytical model for the prediction of solar cell temperature for a high-concentration photovoltaic system, Case Stud. Therm. Eng. 25 (2021) 100890, https://doi.org/10.1016/j.csite.2021.100890.
[6] D.M. Atia, A.A. Hassan, H.T. El-Madany, A.Y. Eliwa, M.B. Zahran, Degradation and energy performance evaluation of mono-crystalline photovoltaic modules in Egypt, Sci. Rep. 13 (1) (2023) 13066, https://doi.org/10.1038/s41598-023-40168-8.
[7] A. El Hammoumi, S. Chtita, S. Motahhir, A. El Ghzizal, Solar PV energy: from material to use, and the most commonly used techniques to maximize the power output of PV systems: a focus on solar trackers and floating solar panels, Energy Rep. 8 (2022) 11992–12010, https://doi.org/10.1016/j.egyr.2022.09.054.
[8] M. Koehl, M. Heck, S. Wiesmeier, J. Wirth, Modeling of the nominal operating cell temperature based on outdoor weathering, Sol. Energy Mater. Sol. Cells 95 (7) (2011) 1638–1646, https://doi.org/10.1016/j.solmat.2011.01.020.
[9] A. Luque, S. Hegedus (Eds.), Handbook of Photovoltaic Science and Engineering, John Wiley & Sons, The Atrium, Southern Gate, Chichester, West Sussex PO19 8SQ, England, 2011.
[10] P. Kamkird, N. Ketjoy, W. Rakwichian, S. Sukchai, Investigation on temperature coefficients of three types photovoltaic module technologies under Thailand operating condition, Procedia Eng. 32 (2012) 376–383, https://doi.org/10.1016/j.proeng.2012.01.1282.
[11] L. Alhmoud, Why does the PV solar power plant operate Ineffectively? Energies 16 (10) (2023) 4074, https://doi.org/10.3390/en16104074.
[12] F. Esmaeilion, M. Soltani, J. Nathwani, A. Al-Haq, Design, analysis, and optimization of a novel poly-generation system powered by solar and wind energy, Desalination 543 (2022) 116119, https://doi.org/10.1016/j.desal.2022.116119.
[13] Y. Fenga, W. Haoa, H. Lia, N. Cuib, D. Gonga, L. Gao, Machine learning models to quantify and map daily global solar radiation and photovoltaic power, Renew. Sustain. Energy Rev. 118 (2020) 1093, https://doi.org/10.1016/j.rser.2019.109393.
[14] Z. Wang, Z. Wang, Q. Li, Forecasting the industrial solar energy consumption using a novel seasonal GM(1,1) model with dynamic seasonal adjustment factors, At. Energ. 200 (2020) 117460, https://doi.org/10.1016/j.energy.2020.117460.
[15] F. Esmaeilion, M. Soltani, J. Nathwani, Assessment of a novel solar-powered polygeneration system highlighting efficiency, exergy, economic and environmental factors, Desalination 540 (2022) 116004, https://doi.org/10.1016/j.desal.2022.116004.
[16] C. Schwingshackl, M. Petitta, J.E. Wagner, G. Belluardo, D. Moser, M. Castelli, A. Tetzlaff, Wind effect on PV module temperature: analysis of different techniques for an accurate estimation, Energy Proc. 40 (2013) 77–86, https://doi.org/10.1016/j.egypro.2013.08.010.
[17] M. Mattei, G. Notton, C. Cristofari, M. Muselli, P. Poggi, Calculation of the polycrystalline PV module temperature using a simple method of energy balance, Renew. Energy 31 (4) (2006) 553–567, https://doi.org/10.1016/j.renene.2005.03.010.
[18] T.A. Olukan, M. Emziane, A comparative analysis of PV module temperature models, Energy Proc. 62 (2014) 694–703, https://doi.org/10.1016/j.egypro.2014.12.433.
[19] D.P.N. Nguyen, K. Neyts, J. Lauwaert, Proposed models to improve predicting the operating temperature of different photovoltaic module technologies under various Climatic conditions, Appl. Sci. 11 (15) (2021) 7064, https://doi.org/10.3390/app11157064.
[20] E. Barykina, A. HammerModeling of photovoltaic module temperature using Faiman model: sensitivity analysis for different climates, Sol. Energy 146 (2017) 401–416. https://10.1016/j.solener.2017.03.002.
[21] E.M. Brito, A.F. Cupertino, P.D. Reigosa, Y. Yang, V.F. Mendes, H.A. Pereira, Impact of meteorological variations on the lifetime of grid-connected PV inverters, Microelectron. Reliab. 88 (2018) 1019–1024, https://doi.org/10.1016/j.microrel.2018.07.066.
[22] R. Ayaz, I. Nakir, M. Tanrioven, An improved Matlab-Simulink model of PV module considering ambient conditions, Int. J. Photoenergy INT. J. PHOTOENERGY 2014 (2014), https://doi.org/10.1155/2014/315893. Article ID 315893.
[23] E.B. Agyekum, S. PraveenKumar, N.T. Alwan, V.I. Velkin, S.E. Shcheklein, S.J. Yaqoob, Experimental investigation of the effect of a combination of active and passive cooling mechanism on the thermal characteristics and efficiency of solar PV module, Invention 6 (4) (2021) 63, https://doi.org/10.3390/inventions6040063.
[24] M. Akhsassi, A. El Fathi, N. Erraissi, N. Aarich, A. Bennouna, M. Raoufi, A. Outzourhit, Confrontation à l'expérience de divers modèles du comportement thermique de modules solaires photovoltaïques, 4ème Congr, l'Association Marocaine Therm (2016) 1–7, https://doi.org/10.13140/RG.2.2.28352.35846.
[25] J.K. Kaldellis, M. Kapsali, K.A. Kavadias, Temperature and wind speed impact on the efficiency of PV installations: Experience obtained from outdoor measurements in Greece, Renew. Energy 66 (2014) 612–624, https://doi.org/10.1016/j.renene.2013.12.041.
[26] C.F. Abe, J.B. Dias, G. Notton, G.A. Faggianelli, Experimental application of methods to compute solar irradiance and cell temperature of photovoltaic modules, Sensor 20 (9) (2020) 2490, https://doi.org/10.3390/s20092490.
[27] M. Zouine, M. Akhsassi, N. Erraissi, N. Aarich, A. Bennouna, M. Raoufi, A. Outzourhit, Mathematical models calculating PV module temperature using weather data: experimental study, in: Int. Conf. Power Eng. Renew. Energy ICEERE 2018, 15-17 April 2018, Saidia, Morocco 1, Springer Singapore, 2019, pp. 630–639, https://doi.org/10.1007/978-981-13-1405-6_72.
[28] M. Muneeshwaran, U. Sajjad, T. Ahmed, M. Amer, H.M. Ali, C.C. Wang, Performance improvement of photovoltaic modules via temperature homogeneity improvement, Energy 203 (2020) 117816, https://doi.org/10.1016/j.energy.2020.117816.
[29] S.A. Kalogirou, Solar Energy Engineering: Processes and Systems, Academic press, 2013. https://www.researchgate.net/publication/41117169.
[30] D.T. Cotfas, P.A. Cotfas, O.M. Machidon, Study of temperature coefficients for parameters of photovoltaic cells, INT. J. PHOTOENERGY 2018 (2018), https://doi.org/10.1155/2018/5945602. Article ID 5945602.
[31] R. Araneo, U. Grasselli, S. Celozzi, Assessment of a practical model to estimate the cell temperature of a photovoltaic module, Int. J. Energy Environ. Eng. 5 (2014) 1–16, https://doi.org/10.1007/s40095-014-0072-x.
[32] E.P.J.A. Skoplaki, J.A. Palyvos, Operating temperature of photovoltaic modules: a survey of pertinent correlations, Renew. Energy 34 (1) (2009) 23–29, https://doi.org/10.1016/j.renene.2008.04.009.
[33] S. Kichou, N. Skandalos, P. Wolf, Floating photovoltaics performance simulation approach, Heliyon 8 (12) (2022) e11896, https://doi.org/10.1016/j.heliyon.2022.e11896.
[34] L.T. Scarabelot, G.A. Rampinelli, C.R. Rambo, Overirradiance effect on the electrical performance of photovoltaic systems of different inverter sizing factors, J. Sol. Energy 225 (2021) 561–568, https://doi.org/10.3390/app13053155.
[35] X.J. Dong, J.N. Shen, G.X. He, Z.F. Ma, Y.J. He, A general radial basis function neural network assisted hybrid modeling method for photovoltaic cell operating temperature prediction, Energy 234 (2021) 121212, https://doi.org/10.3390/jmse9111231.
[36] S. Al-Dahidi, S. Al-Nazer, O. Ayadi, S. Shawish, N. Omran, Analysis of the effects of cell temperature on the predictability of the solar photovoltaic power production, IJEEP 10 (5) (2020) 208, https://doi.org/10.32479/ijeep.9533.
[37] R. Ndegwa, E. Ayieta, J. Simiyu, N. Odero, A simplified simulation procedure and analysis of a photovoltaic solar system using a single diode model, J. Energy Power Eng. (2020), https://doi.org/10.4236/jpee.2020.89006.
[38] S.N. Nnamchi, M.M. Mundu, Development of solar isodose lines: mercatorian and spatial guides for mapping solar installation areas, beliyon 8 (10) (2022), https://doi.org/10.1016/j.heliyon.2022.e11045.
[39] UETCL, Electricity transmission for Sustainable regional development. https://uetcl.go.ug, 2023. (Accessed 14 April 2023).

[40] S.N. Nnamchi, Z.O. Jagun, O.A. Nnamchi, M.M. Mundu, U. Onochie, Modelling and simulation of wind flow: a gradient method of identifying windy region, Wind Eng. 47 (5) (2023), https://doi.org/10.1177/0309524X2311787.
[41] UNMA, Uganda national meteorological Authority UNMA, weather-ambient temperature. https://www.unma.go.ug/, 2023. (Accessed 14 July 2022).
[42] D.A. Prasetya, P.T. Nguyen, R. Faizullin, I. Iswanto, E.F. Armay, Resolving the shortest path problem using the haversine algorithm, J. Crit. Rev. 7 (1) (2020) 62–64, https://doi.org/10.22159/jcr.07.01.11. https://www.lppm.unmer.ac.id/webmin/assets/uploads/lj/LJ20210109161016316836 6.pdf.
[43] A. Al-Bashir, Analysis of effects of solar irradiance, cell temperature and wind speed on photovoltaic systems performance, IJEEP 10 (1) (2020) 353–359, https://doi.org/10.32479/ijeep.859.
[44] S.N. Nnamchi, O.A. Nnamchi, E.O. Sangotayo, M.M. Mundu, O.O. Edosa, Design and fabrication of insulation testing rig, IJEMS 16 (2019) 60–79. https://www.researchgate.net/publication/330754616.
[45] O. Living, S.N. Nnamchi, M.M. Mundu, K.J. Ukagwu, A. Abdulkarim, Coupled modelling and simulation of power transmission lines: a systematic analysis of line losses, Electr. Power Syst. Res. 226 (2024) 109954, https://doi.org/10.1016/j.epsr.2023.109954.